IEEE Photonics Journal
An IEEE Photonics Society Publication

Open Access

An Optical Fiber Fabry–Perot Interferometric Sensor Based on Functionalized Diaphragm for Ultrasound Detection and Imaging

Volume 9, Number 3, June 2017

Wenlu Zhang
Ruohui Wang
Qiangzhou Rong
Xueguang Qiao
Tuan Guo
Zhihua Shao
Jiacheng Li
Wenwen Ma

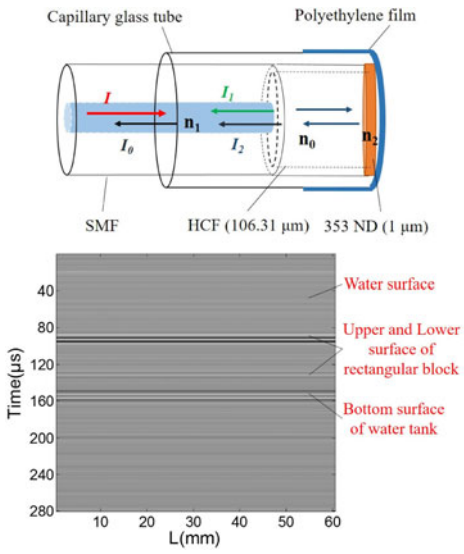

DOI: 10.1109/JPHOT.2017.2694480
1943-0655 © 2017 IEEE

IEEE photonics SOCIETY

IEEE

An Optical Fiber Fabry–Perot Interferometric Sensor Based on Functionalized Diaphragm for Ultrasound Detection and Imaging

Wenlu Zhang,[1] Ruohui Wang,[1] Qiangzhou Rong,[1] Xueguang Qiao,[1] Tuan Guo,[1,2] Zhihua Shao,[1] Jiacheng Li,[1] and Wenwen Ma[1]

[1]School of Physics, Northwest University, Xi'an 710069, China
[2]Guangdong Provincial Key Laboratory of Optical Fiber Sensing and Communications, Institute of Photonics Technology, Jinan University, Guangzhou 510632, China

DOI:10.1109/JPHOT.2017.2694480
1943-0655 © 2017 IEEE. Translations and content mining are permitted for academic research only. Personal use is also permitted, but republication/redistribution requires IEEE permission. See http://www.ieee.org/publications_standards/publications/rights/index.html for more information.

Manuscript received February 27, 2017; revised April 10, 2017; accepted April 11, 2017. Date of publication April 17, 2017; date of current version May 1, 2017. This work was supported in part by the National Natural Science Foundation of China under Grant 61275088, Grant 61505163, and Grant 61327012; in part by Scientific Research Program funded by Shaanxi Provincial Education Department (Program 08JZ58); in part by the Guangdong Youth Science and Technology Innovation Talents of China under Grant 2014TQ01X539; in part by the Guangdong Natural Science Foundation of China under Grant 2014A030313387; and in part by the Guangzhou Key Collaborative Innovation Foundation of China under Grant 2016201604030084. Corresponding author: Ruohui Wang (e-mail: rwang@nwu.edu.cn).

Abstract: A miniature optical fiber ultrasonic sensor based on the Fabry–Perot interferometer (FPI) is proposed and experimentally demonstrated. The cavity of the interferometer is based on a section of hollow core fiber coated with a 353ND diaphragm. A well-define interference pattern is achieved, and the spectral sideband filter technique is used to interrogate the sensor. Because the thin reflective diaphragm is extremely sensitive to sound pressure, the signal-to-noise ratio of the sensor response reaches to 31.22 dB with the pulse ultrasonic excitation of 300 kHz. A clear interface information can be distinguished in physical model imaging, and the longitudinal spatial resolution is 5 mm. This proposed sensor has the advantages of being simple to fabricate, ultracompact in size, cost effective, corrosion resistance, and being highly stable.

Index Terms: Optical fiber sensor, Fabry–Perot interferometer (FPI), sensor fabrication, ultrasonic measurement.

1. Introduction

Ultrasonic detection and imaging technology has a wide applications in structural health monitoring [1], ultrasonic surgery [2], oil well logging [3], etc. The ultrasonic image can provide a visual information, which directly reflects the structural information and mechanical properties of the target. The detection of ultrasound is commonly achieved by using piezoelectric transducers (PZTs) [4], [5]. However, the material of PZT is sensitive to electromagnetic interference, which causes signal distortion due to the electrical loading effects. Performance degradation in the harsh environment also limits its real application.

The optical fiber sensor, with features of high sensitivity, electromagnetic interference immunity, and multiplex capability, has been widely used to detect ultrasound. Fiber gratings [6], fiber

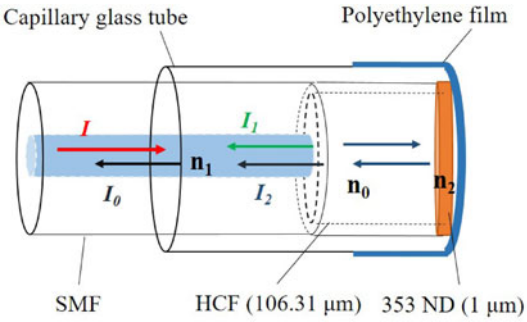

Fig. 1. Schematic diagram of the sensor.

interferometers [7], [8], Fiber tapers [9], couplers [10], and fiber lasers [11] have been proposed for ultrasonic sensing. A Fabry-Perot interferometer (FPI) based ultrasonic sensor is generally composed of a thin film as diaphragm and an optical fiber end-face as two reflectors. The diaphragm will vibrate under the effect of ultrasound, which induce the cavity length changes and eventually leads to the shift of the interferometer spectrum. A wide variety of diaphragm based FPI ultrasonic sensors have been proposed. *Ma et al.* proposed a FPI based acoustic sensor with multilayer graphene diaphragms [12], [13]. The sensor has a pressure sensitivity up to 1100 nm/kPa and is able to detect acoustic signals as small as 60 μPa/$\sqrt{Hz}$ at 10 kHz. However, the preparation of graphene film is quite complicated which limits the sensor's application. Metal diaphragms have also been used to detect ultrasound. For example, *Xu et al.* proposed an optical fiber acoustic pressure sensor based on a large-area nanolayer silver diaphragm [14]. The sensor exhibits a high dynamic pressure sensitivity of 160 nm/Pa at 4 kHz and a detectable pressure level of 14.5 μPa/$\sqrt{Hz}$. However, the large Young's modulus and small resonance frequency of the metal diaphragms induce the low ultrasonic response. Polymer membranes such as polyethylene terephthalate film [15] and Parylene-C [16] are also used to fabricate FPI based ultrasonic sensor. However, polymer materials have poor chemical stability and heat resistance.

In this paper, we propose and experimentally demonstrate a highly sensitive optical fiber FPI based ultrasonic sensor. The sensor is based a section of hollow core fiber (HCF) coated with a 353ND diaphragm. Spectral sideband filter technique is used to interrogate the sensor and a high ultrasonic response with high signal to noise ratio (SNR) is achieved. The proposed sensor is applied in physical model imaging and a clear interface information can be differentiated. The use of 353ND gives the FPI the capability to detect ultrasound in a harsh environment.

2. Sensor Fabrication and Operation Principle

The structure schematic diagram of the sensor is shown in Fig. 1. The fabrication of the sensor involves four steps: First, a HCF with a core diameter of 100 μm is spliced to a single mode fiber (SMF) and then cleaved into a section of 106.31 μm. Second, the HCF is dipped into 353ND adhesive (353ND is a two-component thermosetting epoxy resin adhesive, which is developed by EPOXY Technology Inc. The two components are mixed with the weight proportion of 10:1. It can work continuously in the temperature range of $-55 \sim 250$ °C and can work for several minutes in 300$\sim$400 °C, and has excellent resistance for a variety of solvents and chemicals.) which is often used for optical fiber and related device adhesion [17]. Compared with other coating process such as unbalanced magnetron sputtering technology, using this method to coat 353ND film is simple to operate and cost effective. Then, to make the epoxy curing, the fiber tip is heated at 80 °C for 15 min. After curing, the 353ND epoxy resin adhesive forms a smooth diaphragm at the end face of HCF. In the package step, a capillary glass tube with inner diameter of 0.3 mm and a polyethylene film are used to isolate water. Since ultrasound also causes vibration of the polyethylene film, the 353ND

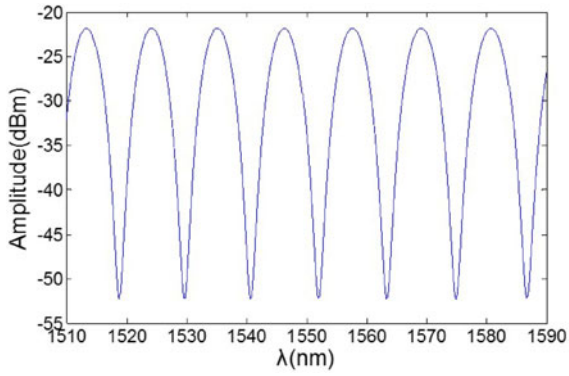

Fig. 2. Numerical simulation result of the sensor's reflective spectrum.

diaphragm and the polyethylene film are separated by a proper distance to avoid the influence on the sensor's spectrum.

One advantage of using the 353ND as the diaphragm is that the material is resistant to high temperature and the sensor can be operated in a high temperature environment up to 250 °C. In addition, the Young's modulus of 353ND (∼1 GPa) is much lower than other materials such as polymers (4∼5 GPa), fused-silica fiber (70 GPa) and metals (Tens to hundreds GPa), which improve the acoustic response of the proposed sensor.

Two reflections form the cavity of the FPI: One is SMF-air interface and another is the 353ND-air boundary. The Fresnel reflection coefficients arising from the refractive index mismatches at the boundaries are low and thus the multiple reflections within the interferometer can be neglected. Therefore, the principle of the interferometer can be modeled by two beams interference theory.

When the interferometer is illuminated with light, the resultant intensity I_0 owing to the interference of I_1 and I_2 from the two reflections of the FPI can be expressed as

$$I_0 = I_1 + I_2 + 2\sqrt{I_1 I_2}\cos\Phi \tag{1}$$

$$I_1 = I R_1 \tag{2}$$

$$I_2 = I(1 - R_1)^2 R_2 \tag{3}$$

where Φ is the total phase difference arising from the optical path length difference between the two reflections. R_1 and R_2 are the reflectivity and can be expressed as

$$R_1 = \left(\frac{n_0 - n_1}{n_0 + n_1}\right)^2, R_2 = \frac{R[2(1-R)\cos\Phi_1 + (1-R)^2 + 1]}{1 - R_1} \tag{4}$$

where $R = [(n_2 - n_0)/(n_2 + n_0)]^2$ is the reflectivity of the inner and outer surfaces of 353ND film. Φ_1 is the phase difference between the two reflections of inner and outer surfaces of 353ND film. And n_0, n_1, n_2 are the refractive index of air, core of SMF and 353ND, respectively. When only considering vertical incidence, the phase differences can be expressed as

$$\Phi = \frac{2\pi}{\lambda} \cdot \left(2n_0 l + \frac{\lambda}{2}\right) \tag{5}$$

$$\Phi_1 = \frac{2\pi}{\lambda} \cdot \left(2n_2 d + \frac{\lambda}{2}\right) \tag{6}$$

where l is the FPI cavity length. d is the thickness of 353ND film. λ is the wavelength of the laser, and $\lambda/2$ is the half wave loss at air/film interface. The numerical simulation result of the sensor's reflective spectrum is shown in Fig. 2 . It can be seen that the sensor has a desired spectrum.

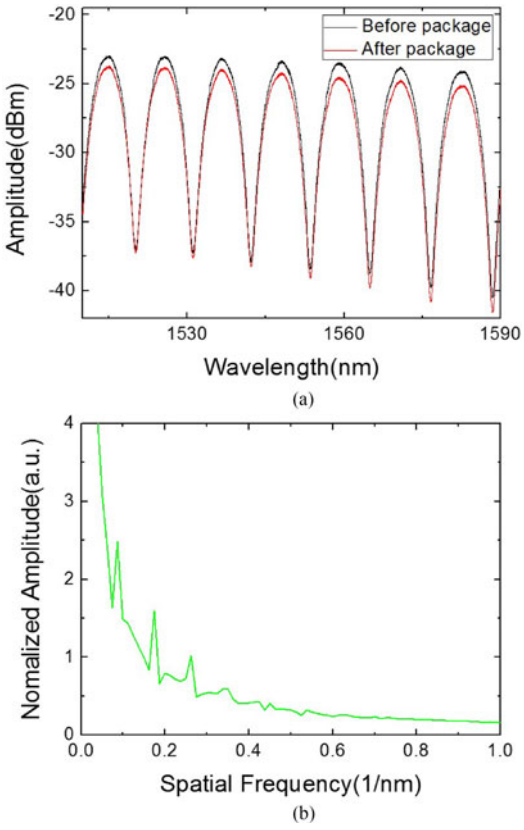

Fig. 3. (a) Interference spectra at room temperature. (b) Spatial frequency spectrum.

A normally incident ultrasound will lead to the vibration of 353ND film and the change of film thickness, which then gives rise to a phase shift Φ

$$\Phi = \varphi + d\varphi \tag{7}$$

$$d\varphi = \frac{4\pi n_0 dl}{\lambda} \tag{8}$$

where the phase-bias term φ defines the working point of the interferometer and the time-varying signal term dφ arises from the ultrasonic induced change of the cavity length *dl*. When the frequency of the ultrasound is equal to the natural frequency of the diaphragm, *dl* reaches to its maximum, and the natural frequency of the 353ND diaphragm can be calculated as [18]

$$f_0 = \frac{10.33h}{2\pi r^2}\sqrt{\frac{E}{12\rho(1-\mu^2)}} \tag{9}$$

where h, r, ρ, μ, and E are the thickness, radius, density, Poisson ratio, and Young's modulus of the diaphragm, respectively. The natural frequency is calculated to be 5.97 MHz when these parameters are 1 μm, 50 μm, 1.18 kg/m^3, 0.38 and 1 GPa, respectively. It can be seen that the sensor has a larger resonance frequency compared to with that in [12]–[14].

3. Experiment and Discussion

Fig. 3(a) presents typical reflective spectra of the sensor before and after packaging. The spectrum after packaging has a max extinction ratio of 17.8 dB and a free spectral range (FSR) of 11.5 nm,

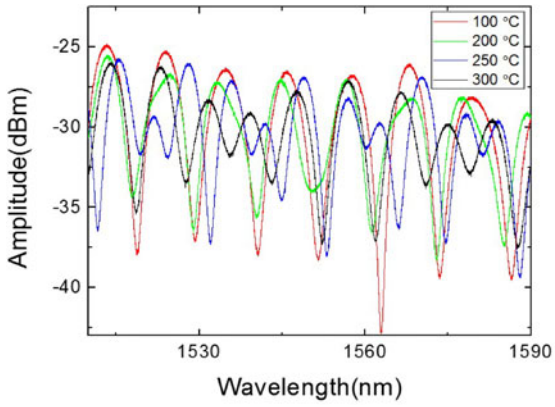

Fig. 4. Sensor's spectrums at different temperatures.

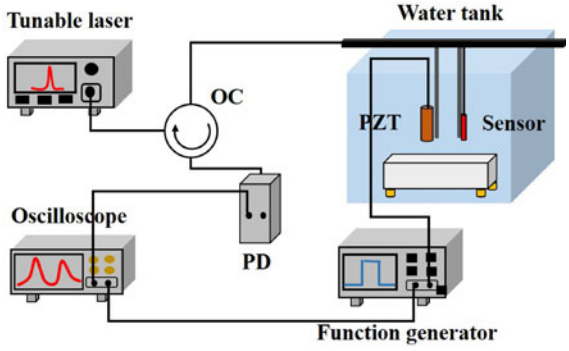

Fig. 5. Schematic diagram of the ultrasonic detection system.

respectively. The effective cavity length (l) of the FPI can be calculated to be 105.67 μm by

$$l = \frac{\lambda_1 \lambda_2}{2n_0(\lambda_2 - \lambda_1)} \tag{10}$$

where λ_1 and λ_2 is the resonant wavelengths of the reflection spectrum. The measured cavity length is 106.31 μm which is close to the calculated one. In the numerical simulation, we neglect the light energy loss in the materials, interference cavity and laboratory apparatus, and therefore the experimental spectrum has larger loss and smaller extinction ratio. In order to analyze the characteristics of the interference patterns, the spectrum of the packaged sensor is transformed to the spatial frequency, which is shown in Fig. 3(b). The peak with low frequency are caused by light interference from the two surface of the 353ND film, which results in the increase of the extinction ratio with the increase of the wavelength.

The sensors temperature response test was preformed to evaluate its temperature resistance capability. As shown in Fig. 4, the FSR of the spectra keep constant and only a small extinction ratio change can be observed with the temperature increasing to 250 °C. When the temperature is higher than 250 °C, the spectral shape changes dramatically, indicating that 353ND film experience a larger deformation. Therefore, the proposed sensor can normally operate in high temperature environment up to 250 °C.

The sideband filter technique is used to interrogate the proposed ultrasonic sensor and the experiment setup for physical model imaging is shown in Fig. 5 . The sideband filter technique has the advantages of simple structure, low cost, and can effectively suppress the fluctuation of the output power of light source. A rectangular Plexiglas block (50 cm $\times$ 50 cm $\times$ 6 cm) is placed in a water tank as a simple physical model. To avoid the superposition of reflection signals from the rectangular Plexiglas block and the bottom surface of the water tank, four copper cylinders (depth of

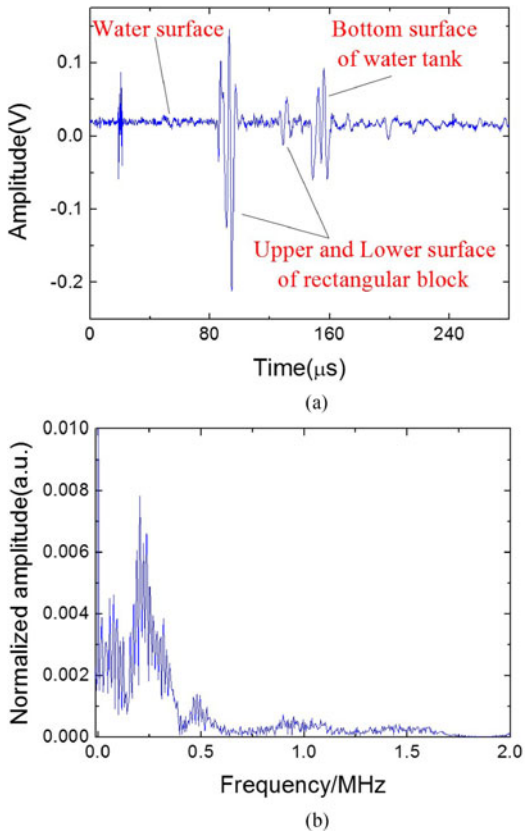

Fig. 6. (a) Real time measurement of response waveform. (b) Spatial frequency result.

1.20 cm) are sandwiched between them. A PZT driven by a pulse square wave is used to generate ultrasound with the frequency of 300 kHz. The PZT and optical fiber sensor are fixed on a scanning platform which is located above the surface of water. The horizontal distance between the sensor and PZT are 5 cm. The optical fiber sensor is illuminated by a tunable laser (Santec, TSL-710) with a line width of 100 kHz and power of 20 mW. A photodetector (PD) is used to convert the light to electrical signal which is recorded by a digital oscilloscope (RIGOL, DS2302A). To obtain the maximum sensitivity response, the laser wavelength is tuned to the 3 dB bandwidth wavelength of one linear side of the interference fringe. When the ultrasound is loaded on the sensor, the cavity length of the FPI will be changed, resulting in the shift of the interference pattern. Spectral sideband filtering method is employed to transfer the spectral shift to the change of optical power. Then the change in optical power is converted to a voltage signal by a PD, which is displayed on an oscilloscope.

Fig. 6 (a) shows a real-time measurement of the response waveform. The horizontal axis and vertical axis represent ultrasonic propagation time in water and the signal response amplitude, respectively. In the result, the direct wave from the water surface, the reflected wave from the upper and lower surface of the rectangular Plexiglas block, and the bottom surface of the water tank can be clearly distinguished. Owing to the diagram's high sensitive to the sound pressure, the sensor obtains a signal peak value of 364 mV and the noise is only 10 mV, resulting in a SNR of 31.22 dB. In our test, the ultrasonic velocities are 1473 m/s and 2692 m/s in water and rectangular Plexiglas block, respectively. The travel time of the ultrasonic reflected waves can be calculated to be 87.89 μs, 132.47 μs and 148.76 μs, which is in accordance with the result shown in Fig. 6(a). To further analyze the temporal response, the time domain signal is transformed to the spatial frequency, as shown in Fig. 6(b). It can be seen that the main frequency response of the sensor is close to 300 kHz and the ultrasonic frequency is consistent with the resonance frequency of PZT.

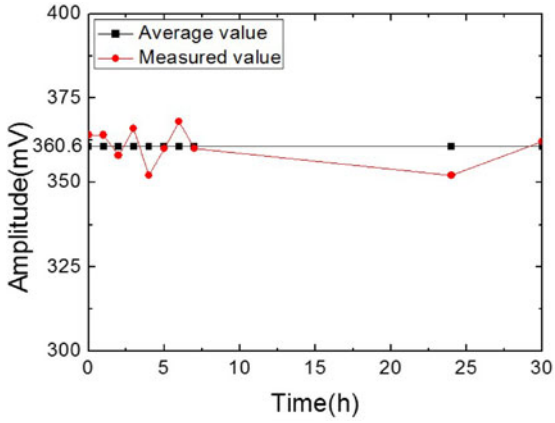

Fig. 7. Stability test of the sensor.

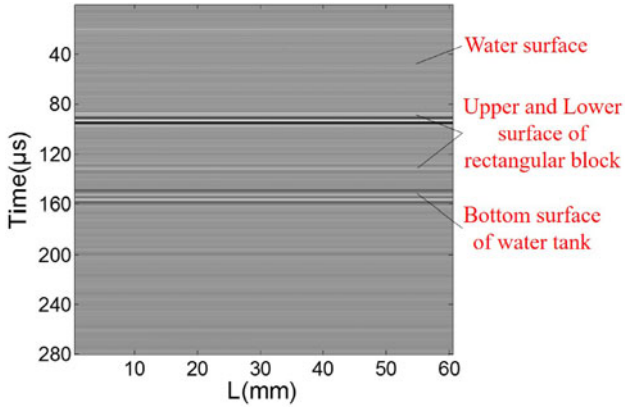

Fig. 8. Ultrasonic imaging of the physical model.

Besides the high sensitivity and SNR, the stability of the sensor is also one of the important factors for the physical model imaging and other practical applications. In general, the stability is affected by the interference of the external environment induced spectral drift. Fig. 7 shows the sensitivity fluctuations of the sensor over 30 hours. It can be seen that the maximum fluctuation of the ultrasonic response just only 8.6 mV, which is small compared with the average value 360.6 mV. It indicates that the proposed ultrasonic sensor is stable in long-term measurement.

The proposed sensor is also experimentally demonstrated for the physical model scanning and imaging. The seismic physical model is used to simulate the real geological structure in laboratory, which is much cost-effective and more repeatable compared to experiments in the field. The horizontal distance between the sensor and PZT is also set to be 5 cm. The sensor and PZT are programmed to move along the water surface with a step of 1 mm and the total scanning range is 6 cm. The waveform data are manually stored on the oscilloscope after the scanning platform automatically moves one step. Completing one scanning of the 2-D image if a physical model takes ~8 minutes. Fig. 8 shows the ultrasonic image reconstructed by time-of-flight approach using our imaging system. The horizontal axis and vertical axis represent the transverse length of the physical model and ultrasonic propagation time, respectively. Four layers involving the water surface, upper and lower surfaces of the rectangular Plexiglas block and the bottom surface of the water tank can be clearly observed. The topside signal is the location of the sensor and PZT in the vertical direction. The position of each layer is also consistent with the ultrasonic reflection time of Fig. 6(a) and the actual situation. Thanks to the good ultrasonic response of the proposed sensor, the signal of the diffraction wave at the interface of each material can be collected. Knowing the ultrasonic

propagation time and velocity, the longitudinal spatial resolution of the sensor can be calculated to be 5 mm.

4. Conclusion

We propose and experimentally demonstrate a FPI based ultrasonic sensor for physical model imaging. The sensor is based on the 353ND diaphragm, which can be used in high temperature environment. A clear interference pattern with a max extinction ratio of 17.8 dB and an FSR of 11.5 nm is obtained. The spectral sideband filter technique is used to interrogate the sensor and an SNR of 31.22 dB is obtained with the pulse ultrasonic excitation of 300 kHz. A longitudinal spatial resolution of 5 mm is obtained in physical model imaging. The proposed sensor is simple to fabricate, ultra-compact in size, cost effective, and highly stable. In harsh environment applications, it can replace the use of piezoelectric devices as a miniature and flexible probe sensor.

References

[1] Y. Lu and J. E. Michaels, "Feature extraction and sensor fusion for ultrasonic structural health monitoring under changing environmental conditions," *IEEE Sensors J.,* vol. 9, no. 11, pp. 1462–1471, Nov. 2009. [Online]. Available: http://www.quest.gatech.edu/publications/journals/Lu_IEEESensor2009_SurfaceWetting.pdf

[2] R. M. Gruber *et al.*, "Ultrasonic surgery—An alternative way in orthognathic surgery of the mandible. A pilot study," *Int. J. Oral Maxillofacial Surg.*, vol. 34, no. 6, pp. 590–593, 2005. [Online]. Available: https://doi.org/10.1016/j.ijom.2005.06.006

[3] R. M. Havira, "Ultrasonic techniques in oil well logging," in *Proc. IEEE Ultrason. Symp.,* 1986, vol. 34, pp. 563–572, 1988. Available: http://ieeexplore.ieee.org/document/1535741/

[4] K. Toda and A. Sawaguchi, "Ultrasonic imaging system using a leaky surface acoustic wave transducer composed of piezoelectric ceramic and fused quartz," *J. Appl. Phys.,* vol. 69, no. 1, pp. 103–108, 1991. [Onlline]. Available: http://doi.org/10.1063/1.347745

[5] F. Levassort, M. P. Thi, and P. Marechal, "Ultrasonic transducer based on highly textured PMN-PT piezoelectric ceramic," *J. Electroceram.,* vol. 19, no. 4, pp. 375–381, 2007. [Onlline]. Available: https://doi.org/10.1007/s10832-007-9176-5

[6] G. Wild and S. Hinckley, "Acousto-ultrasonic optical fiber Sensors: Overview and state-of-the-art acousto-ultrasonic optical fiber Sensors: Overview and state-of-the-art," *IEEE Sensor J.*, vol. 8, no. 7, pp. 1184–1193, Jul. 2008. [Online]. Available: http://ieeexplore.ieee.org/document/4567505/

[7] J. Ma, Y. Yu, and W. Jin, "Demodulation of diaphragm based acoustic sensor using Sagnac interferometer with stable phase bias," *Opt. Exp.,* vol. 23, no. 22, pp. 29268–29278, 2015. [Online]. Available: https://doi.org/10.1364/OE.23.029268

[8] D. Gallego, D. Saéz-Rodriguéz, D. Webb, O. Bang, H. Lamela, and L. T. Group, "Interferometric microstructured polymer optical fiber ultrasound sensor for optoacoustic endoscopic imaging in biomedical applications," *Proc. SPIE*, vol. 9157, 2014, Art. no. 91574X. [Online]. Available: https://doi.org/10.1117/12.2059290

[9] B. Xu, Y. Li, M. Sun, Z. Zhang, X. Dong, and S. Jin, "Acoustic vibration sensor based on nonadiabatic tapered fibers," *Opt. Lett.,* vol. 37, no. 22, pp. 4768–4770, 2012. [Online]. Available: https://doi.org/10.1364/OL.37.004768

[10] R. Chen, G. Fernando, T. Butler, and R. A. Badcock, "A novel ultrasound fibre optic sensor based on a fused-tapered optical fibre coupler," *Meas. Sci. Technol.,* vol. 15, no. 8, pp. 1490–1495, 2004. [Online]. Available: https://doi.org/10.1088/0957-0233/15/8/010

[11] S. Foster, A. Tikhomirov, and M. Milnes, "A fiber laser hydrophone," *Proc. SPIE,* vol. 5855, pp. 627–630, 2005. [Online]. Available: https://doi.org/10.1117/12.623273

[12] J. Ma, W. Jin, H. Ho, and J. Y. Dai, "High-sensitivity fiber-tip pressure sensor with graphene diaphragm," *Opt. Lett.,* vol. 37, no. 13, pp. 2493–2495, 2012. [Online]. Available: https://doi.org/10.1364/OL.37.002493

[13] J. Ma, H. Xuan, H. Ho, and W. Jin. "Fiber-optic Fabry–Perot acoustic sensor with multilayer graphene diaphragm," *IEEE Photon. Technol. Lett.,* vol. 25, no. 10, pp. 932–935, May 2013. [Online]. Available: http://ieeexplore.ieee.org/document/6493391/

[14] F. Xu, J. Shi, K. Gong, H. Li, R. Hui, and B. Yu, "Fiber-optic acoustic pressure sensor based on large-area nanolayer silver diaghragm," *Opt. Lett.,* vol. 39, no. 10, pp. 2838–2840, 2014. [Online]. Available: https://doi.org/10.1364/OL.39.002838

[15] P. C. Beard and T. N. Mills, "Extrinsic optical-fiber ultrasound sensor using a thin polymer film as a low-finesse Fabry–Perot interferometer," *Appl. Opt.,* vol. 35, no. 4, pp. 663–675, 1996. [Online]. Available: https://doi.org/10.1364/AO.35.000663

[16] P. Morris, A. Hurrell, A. Shaw, E. Zhang, and P. Beard, "A Fabry–Perot fiber-optic ultrasonic hydrophone for the simultaneous measurement of temperature and acoustic pressure," *J. Acoust. Soc. Amer.,* vol. 125, no. 6, pp. 3611–3622, 2009. [Online]. Available: https://doi.org/10.1121/1.3117437

[17] Q. Rong, H. Sun, X. Qiao, J. Zhang, M. Hu, and Z. Feng, "A miniature fiber-optic temperature sensor based on a Fabry–Perot interferometer," *J. Opt.,* vol. 14, no. 4, 2012, Art. no. 45002. [Online]. Available: https://doi.org/10.1088/2040-8978/14/4/045002

[18] S. Wang, P. Lu, L. Liu, and H. Liao, "An infrasound sensor based on extrinsic fiber-optic Fabry–Perot interferometer structure," *IEEE Photon. Technol. Lett.,* vol. 28, no. 11, pp. 1–1, Jun. 2016. [Online]. Available: http://ieeexplore.ieee.org/document/7426354/